ITTC Quality System Manual Recommended Procedures and Guidelines

Uncertainty Analysis in CFD, Examples for Resistance and Flow

Maki K., Zhao F., Horn P., Banks J., Martio J., Starke B., Zaghi S., Villa D., Vitola M., Yoon H. S., Jiang Y., Shingo S.

7.5	Process Control
7.5-03	CFD
7.5-03-02	Resistance and Flow
7.5-03-02-01	Uncertainty Analysis in CFD, Examples for Resistance and Flow

Disclaimer

Updated / Edited by	Approved
Specialist Committee on Combined CFD/EFD Methods of 30th ITTC	30th ITTC 2024
Date 06/2024	Date 09/2024
© 2024 ITTC.A Switzerland	DOI:

Table of contents

Abstract

Example results of verification and validation are presented for a single CFD code and for specified objective, geometry, conditions, and available benchmark information. The objectives are to demonstrate the usefulness of QM 7.5-03-01-01 and to establish the levels of verification and validation of simulation results for an established benchmark for ship hydrodynamics CFD validation.

Uncertainty Analysis in CFD, Examples for Resistance and Flow

1. PURPOSE OF PROCEDURE

Provide an example for the verification and validation methodology for a RANS CFD Code and results for steady flow for a cargo/container ship following the Quality Manual procedures 7.5-03-01-01, "Uncertainty Analysis in CFD, Uncertainty Assessment Methodology" and 7.5-03-01-02, "Uncertainty Analysis in CFD, Guidelines for RANS Codes," which are based on the GUM (JCGM, 2008)

2. EXAMPLE FOR RANS CFD CODE

Example results of verification and validation are presented for a single CFD code and for specified objectives, geometry, conditions, and available benchmark in-formation. The CFD code is CFDSHIP-IOWA, which is a general-purpose, multi-block, high performance computing (parallel), unsteady RANS code (Paterson et al, 1998; Wilson et al., 1998) developed for computational ship hydrodynamics. The RANS equations are solved using higher-order upwind finite differences, PISO, $k-\omega$ turbulence model, and exact and approximate treatments, respectively, of the kinematic and dynamic free-surface boundary conditions. The objectives are to demonstrate the usefulness of the proposed verification and validation procedures and methodology and establish the levels of verification and validation of the simulation results for an established benchmark for ship hydrodynamics CFD validation. The section references are to QM procedure 7.5-03-01-01 and the equation numbering is contiguous with QM procedure 7.5-03-01-01.

2.1 Geometry, Conditions, and Benchmark Data

The geometry is the Series 60 cargo/container ship. The Series 60 was used for two of the three test cases at the last international workshop on validation of ship hydrodynamics CFD codes (CFD Workshop Tokyo, 1994). The conditions for the calculations are Froude number Fr = 0.316, Reynolds number Re = 4.3x10^6, and zero sinkage and trim. These are the same conditions as the experiments, except the resistance and sinkage and trim tests, as explained next. The variables selected for verification and validation are resistance CT (integral variable) and wave profile ζ (point variable).

The benchmark data is provided by Toda et al. (1992), which was also the data used for the Series 60 test cases at the CFD Workshop Tokyo (1994). The data includes resistance and sinkage and trim for a range of Fr for the model free condition (i.e., free to sink and trim); and wave profiles, near-field wave pattern, and mean velocities and pressures at numerous stations from the bow to the stern and near wake, all for Fr = (0.16, 0.316) and the zero sinkage and trim model fixed condition. The data also includes uncertainty estimates, which were recently confirmed/updated by Longo and Stern (1999) closely following standard procedures (Coleman and Steele, 1999).

The resistance is known to be larger for free vs. fixed models. Data for the Series 60 indicates about an 8% increase in C_T for the free vs. fixed condition over a range of Fr including Fr=0.316 (Ogiwara and Kajitani, 1994). The Toda et al.

(1992) resistance values were calibrated (i.e., reduced by 8%) for effects of sinkage and trim for the present comparisons.

2.2 Computational Grids

Grid studies were conducted using four grids (m=4), which enables two separate grid studies to be performed and compared. Grid study 1 gives estimates for grid errors and uncertainties on grid 1 using the three finest grids 1-3 while grid study 2 gives estimates for grid errors and uncertainties on grid 2 using the three coarsest grids 2-4. The results for grid study 1 are given in detail and the differences for grid study 2 are also mentioned. The grids were generated using the commercial code GRIDGEN (Pointwise, Inc.) with consideration to topology; number of points and grid refinement ratio r_G; near-wall spacing and k-ω turbulence model requirement that first point should be at y^+<1; bow and stern spacing; and free-surface spacing.

The topology is body-fitted, H-type, and single block. The sizes of grids 1 (finest) through 4 (coarsest) are 101x26x16 = 42,016, 144x36x22 = 114,048, 201x51x31 = 317,781, and 287x78x43 = 876,211 and the grid refinement ratio $r_G = \sqrt{2}$. Clustering was used near the bow and stern in the ξ–direction, at the hull in the η-direction, and near the free surface in the ζ-direction. The y^+ values for grids 1-4 were about 0.7, 1, 1.4, and 2, respectively. About twice the number of grid points in the η-direction would be required to achieve $y^+ < 1.0$ for grids 1-4 (i.e., roughly 1,800,000 points on the finest grid). With grid refinement ratio $r_G = \sqrt{2}$, only grids 1 and 2 were generated. Grids 3 and 4 were obtained by removing every other point from grids 1 and 2, respectively (i.e., the grid spacing of grids 3 and 4 is twice that of grids 1 and 2, respectively). Grids 1 and 2 were generated by specifying the grid spacing at the corners and number of points along the edges of the computational blocks. The faces of the computational blocks were smoothed using an elliptic solver after which the coordinates in the interior were obtained using transfinite interpolation from the block faces. Grid 2 was generated from grid 1 by increasing the grid spacing and decreasing the number of computational cells in each coordinate direction at the corners of the blocks by a factor r_G. A comparison of the four grids at the free surface plane is shown in figure 1 along with computed wave elevation contours.

2.3 Verification and Validation of Integral Variable: Resistance

2.3.1 Verification.

Verification was performed with consideration to iterative and grid convergence studies, i.e., $\delta_{SN} = \delta_I + \delta_G$ and $U_{SN}^2 = U_I^2 + U_G^2$.

Iterative convergence was assessed by examining iterative history of ship forces and L2 norm of solution changes summed over all grid points. Figure 2 shows a portion of the iterative history on grid 1. The portion shown represents a computation started from a previous solution and does not reflect the total iterative history. Solution change drops four orders of magnitude from an initial value of about 10^{-2} (not shown) to a final value of 10^{-6}. The variation in C_T is about 0.2%D over the last period of oscillation (i.e., U_I = 0.2%D). Iterative uncertainty is estimated as half the range of the maximum and minimum values over the last two periods of oscillation (see figure 2c). Iterative histories for grids 2-4 show iterative uncertainties of about 0.02, 0.03, and 0.01%D, respectively. The level of iterative uncertainties for grids 2-4 are about two orders of magnitude less than the grid error and uncertainty. The iterative uncertainty for grid 1 is one order of magnitude smaller than the

grid error. For all four grids the iteration errors and uncertainties are assumed to be negligible in comparison to the grid errors and uncertainties for all four solutions (i.e., $\delta_I << \delta_G$ and $U_I << U_G$ such that $\delta_{SN} = \delta_G$ and $U_{SN} = U_G$).

The results from the grid convergence study for C_T are summarized in tables 1 and 2. The solutions for C_T indicate monotonic convergence with $R_G = \varepsilon_{21}/\varepsilon_{32}$=0.58. The first-order RE estimate $\delta_{RE_{G_1}}$, order of accuracy p_G, and correction factor C_G are

$$\delta^*_{RE_{G_1}} = \left(\frac{\varepsilon_{21_G}}{r_G^{p_G}-1}\right) = \left(\frac{0.07x10^{-3}}{(\sqrt{2})^{1.6}-1}\right) = 0.09x10^{-3} \quad (1)$$

$$p_G = \frac{\ln(\varepsilon_{32_G}/\varepsilon_{21_G})}{\ln(r_G)} = \frac{\ln(0.12/0.07)}{\ln(\sqrt{2})} = 1.6 \quad (2)$$

$$C_G = \frac{r_G^{p_G}-1}{r_G^{p_{G_{est}}}-1} = \frac{(\sqrt{2})^{1.6}-1}{(\sqrt{2})^2-1} = 0.74 \quad (3)$$

where p_{est}=p_{th}=2 was used in equation (3). Uncertainty and error estimates are made next both considering C_G as sufficiently less than or greater than 1 and lacking confidence and C_G as close to 1 and having confidence, as discussed in Section 4.3.

For C_G = 0.74 considered as sufficiently less than or greater than 1 and lacking confidence, U_G is estimated and not δ_G

$$U_G = \left|C_G\delta^*_{RE_{G_1}}\right| + \left|(1-C_G)\delta^*_{RE_{G_1}}\right| = 0.07 \times 10^{-3} + 0.02 \times 10^{-3} = 0.09 \times 10^{-3} \quad (4)$$

U_G is 1.8% S_{G_1}.

For C_G = 0.74 considered close to 1 and having confidence, both δ^*_G and U_{G_C} are estimated

$$\delta^*_{G_1} = C_G\delta^*_{RE_{G_1}} = 0.07 \times 10^{-3} \quad (5)$$

$$U_{G_C} = \left|(1-C_G)\delta^*_{RE_{G_1}}\right| = 0.02\times10^{-3} \quad (6)$$

The corrected solution S_C is defined with $S = S_{G_1}$

$$S_C = S_{G_1} - \delta^*_{G_1} = 4.96 \times 10^{-3} \quad (7)$$

$\delta^*_{G_1}$ and U_{G_C} are 1.4% and 0.4% S_C, respectively. In both cases, the level of verification is relatively small <2%.

Table 2 includes results for grid study 2, which are similar to those for grid study 1, but the values are larger by a factor of about 2, except S_C which differs by only 0.4%. Also shown in table 1 are C_P and C_F. C_F comprises about 70% of C_T and also displays convergence; however, C_P indicates oscillatory convergence. Relatively small C_G and oscillatory C_P suggests that the solutions are relatively far from the asymptotic range. Another reason for oscillatory C_P is that different flow phenomena may be resolved for the finer than the coarser grids.

2.3.2 Validation.

Validation is performed using both the simulation prediction S and the corrected simulation prediction S_C, as summarized in table 3. First using S, the comparison error is calculated with $S = S_{G_1}$ as

$$E = D - S = 5.42 \times 10^{-3} - 5.03 \times 10^{-3} = 0.39 \times 10^{-3} = 7.2\%D \quad (8)$$

The validation uncertainty is calculated as

$$U_V = \sqrt{U_{SN}^2 + U_D^2} = 0.17 \times 10^{-3} = 3.1\%D \quad (9)$$

where $U_{SN}=U_G$ = 1.7%D and U_D= 2.5%D. Comparison error $|E| > U_V$ such that the simulation results are not validated. U_{SN} and U_D are of similar order such that reduction in U_V would require reduction of U_D and U_{SN} (e.g., use of finer grids for U_{SN}). E is positive, i.e., the simulation under predicts the data. The trends shown in Table 1 suggest C_p is too small. Presumably modelling errors such as resolution of the wave field and inclusion of effects of sinkage and trim can be addressed to reduce E and validate C_T at U_V=3.1%D; however, the case for this reasoning is stronger when considering the corrected comparison error, as discussed next.

Second using S_C, the corrected comparison error is calculated as

$$E_C = D - S_C = 5.42 \times 10^{-3} - 4.96 \times 10^{-3} = 0.46 \times 10^{-3} = 8.5\%D \quad (10)$$

The validation uncertainty is calculated as

$$U_{V_C} = \sqrt{U_{S_CN}^2 + U_D^2} = 0.14 \times 10^{-3} = 2.6\%D \quad (11)$$

where $U_{S_CN} = U_{G_C} = 0.4\%D$. Here again, $|E_C| > U_{V_C}$ such that the simulation results are not validated. However, validation uncertainty U_{V_C} is relatively small and $U_{S_CN} \ll U_D$ more strongly suggests than was the case for E that E_C is mostly due to modeling errors. Therefore modeling issues should/can be improved to reduce E_C and validate C_T at the reduced level $U_{V_C} = 2.6\%D$ in comparison to equation (9).

The results from grid study 2 are summarized in table 4. The results are similar to those for grid study 1, but E and E_C are smaller and U_V and U_{V_C} are larger.

2.4 Verification and Validation of a Point Variable: Wave Profile

2.4.1 Verification.

Verification for the wave profile was conducted as per that described for the resistance in Section 2.3 with the distinction that a point variable is defined over a distribution of grid points. Interpolation of the wave profile on all grids onto a common distribution is required to compute solution changes. Since calculation of the comparison error E=D-S is required for validation, wave profiles on grids 1-4 are interpolated onto the distribution of the data. The same four grids were used and, here again iteration errors and uncertainties were negligible in comparison to the grid errors and uncertainties for all four solutions, i.e., $\delta_I << \delta_G$ and $U_I << U_G$ such that $\delta_{SN} = \delta_G$ and $U_{SN} = U_G$.

R_G at local maximums and minimums (i.e., x/L = 0.1, 0.4, and 0.65 in figure 3a) and based on L2 norm solution changes both show convergence. The spatial order of accuracy for the wave profile was computed from the L2 norm of solution changes

$$\langle p_G \rangle = \frac{\ln\left(\left\|\varepsilon_{32_G}\right\|_2 / \left\|\varepsilon_{21_G}\right\|_2\right)}{\ln(r_G)} = 1.4 \quad (12)$$

where < > is used to denote a profile-averaged value and $\|\varepsilon\|_2$ denotes the L2 norm of solution change over the N points in the region, 0 < x/L < 1

$$\|\varepsilon\|_2 = \left[\sum_{i=1}^{N} \varepsilon_i^2\right]^{1/2} \quad (13)$$

Correction factor is computed using order of accuracy p_G in equation (12) and $p_{G_{est}} = 2.0$

$$\langle C_G \rangle = \frac{r_G^{\langle p_G \rangle} - 1}{r_G^{p_{G_{est}}} - 1} = \frac{(\sqrt{2})^{1.4} - 1}{(\sqrt{2})^2 - 1} = 0.60 \quad (14)$$

The estimates for order of accuracy and correction factor in equations (12) and (13) were used to estimate grid error and uncertainty for the wave profile at each grid point.

For $<C_G>$ = 0.60 considered as sufficiently less than or greater than 1 and lacking confidence, pointwise values for U_G are estimated and not δ_G. The U_G is estimated as

$$U_G = \left|\langle C_G\rangle\left(\frac{\varepsilon_{21_G}}{r_G^{\langle p_G\rangle}-1}\right)\right| + \left|(1-\langle C_G\rangle)\left(\frac{\varepsilon_{21_G}}{r_G^{\langle p_G\rangle}-1}\right)\right| \quad (15)$$

For $<C_G>$=0.60 considered close to 1 and having confidence, point wise values for both $\delta_G^*$and $U_{G_C}$are estimated

$$\delta_{G_1}^* = \langle C_G\rangle\left(\frac{\varepsilon_{21_G}}{r_G^{\langle p_G\rangle}-1}\right) \quad (16)$$

$$U_G = \left|(1-\langle C_G\rangle)\left(\frac{\varepsilon_{21_G}}{r_G^{\langle p_G\rangle}-1}\right)\right| \quad (17)$$

The S_C at each grid point is calculated as

$$S_C = S_{G_1} - \delta_{G_1}^* \quad (18)$$

The results are summarized in Table 5. The level of verification is similar to that for C_T with slightly higher values. Table 5 includes results for grid study 2, which are much closer to those for grid study 1 than was the case for C_T.

2.4.2 Validation.

Validation of the wave profile is performed using both the simulation prediction S and the corrected simulation prediction S_C. Profile-averaged values for both definitions of the comparison error, validation uncertainty, and simulation uncertainty are given in table 6. Values are normalized with the maximum value for the wave profile ζ_{max}=0.014 and the uncertainty in the data was reported to be 3.7%ζ_{max}. E is nearly validated at about 5%. The trends are similar to those for C_T, except there are smaller differences between the use of E and E_C.

The point comparison error $E=D-S$ is compared to validation uncertainty U_V in figure 3b, while error $E_C=D-S_C$ is compared to validation uncertainty U_V in figure 3d. In the latter case, the validation uncertainty U_V in figure 3d is mostly due to U_D. Much of the profile is validated. The largest errors are at the crests and trough regions, i.e., bow, shoulder, and stern waves.

The results from grid study 2 are summarized in Table 7 and included in Figure 3. The results are similar to those for grid study 1, but both E and E_C and U_V and $U_{V_C}$are larger.

3. REFERENCES

CFD Workshop Tokyo 1994, 1994, Proceedings, Vol. 1 and 2, 1994, Ship Research Institute Ministry of Transport Ship & Ocean Foundation.

Coleman HW and Steele WG, *Experimentation and Uncertainty Analysis for Engineers* (2nd edition), Wiley: New York, NY, 1999.

JCGM, 2008, "Evaluation of measurement data – Guide to the expression of uncertainty in measurement," JCGM 100:2008 GUM 1995 with minor corrections, Joint Committee for Guides in Metrology, Bureau International des Poids Mesures (BIPM), Sèvres, France.

Longo, J. and Stern, F., "Resistance, Sinkage and Trim, Wave Profile, and Nominal Wake and Uncertainty Assessment for DTMB

Model 5512," Proc. 25th ATTC, Iowa City, IA, 24-25 September 1998.

Ogiwara, S. and Kajitani, H., 1994, "Pressure Distribution on the Hull Surface of Series 60 (CB=0.60) Model," Proceedings CFD Workshop Tokyo, Vol. 1, pp. 350-358.

Paterson, E.G., Wilson, R.V., and Stern, F., 1998, "CFDSHIP-IOWA and Steady Flow RANS Simulation of DTMB Model 5415," 1st Symposium on Marine Applications of Computational Fluid Dynamics, McLean, VA, 19-21 May.

Toda, Y., Stern, F., and Longo, J., 1992, "Mean-Flow Measurements in the Boundary Layer and Wake and Wave Field of a Series 60 CB = .6 Model Ship - Part 1: Froude Numbers .16 and .316," Journal of Ship Research, Vol. 36, No. 4, pp. 360-377.

Wilson, R., Paterson, E., and Stern, F., 1998 "Unsteady RANS CFD Method for Naval Combatant in Waves," Proc. 22nd ONR Symposium on Naval Hydro, Washington, DC.

4. KEYWORDS

Uncertainty Analysis, CFD, Verification and Validation, Ship Resistance and Flow

Table 1 Grid convergence study for total C_T, pressure C_P, and frictional C_F resistance ($x10^{-3}$) for Series 60.

Grid	*Grid 4 101x26x16*	*Grid 3 144x36x22*	*Grid 2 201x51x31*	*Grid 1 287x71x43*	*Data*
C_T	5.72	5.22	5.10	5.03	5.42
ε		-8.7%	-2.3%	-1.3%	
C_P	1.95	1.63	1.64	1.61	C_R = 2.00
ε		-16.4%	+0.6%	-1.8%	
C_F	3.78	3.59	3.46	3.42	3.42
ε		-5.0%	-3.6%	-1.2%	ITTC

% of finer grid value.

Table 2. Verification of total resistance C_T ($x10^{-3}$) for Series 60.

Study	R_G	p_G	C_G	U_G	δ_G^*	U_{G_C}	S_C
1 (grids 1-3)	0.57	1.6	0.74	1.8%	1.4%	0.4%	4.96
2 (grids 2-4)	0.24	4.1	3.1	3.9%	2.4%	1.6%	4.98

%SG.

Table 3. Validation of total resistance for Series 60 – study 1 (grids 1-3).

	E%	U_V%	U_D%	U_{SN}%
$E=D-S$	7.2	3.1	2.5	1.7
$E_C=D-S_C$	8.5	2.6	2.5	0.4

%D.

Table 4. Validation of total resistance for Series 60 – study 2 (grids 2-4).

	E%	U_V%	U_D%	U_{SN}%
$E=D-S$	5.9	4.4	2.5	3.7
$E_C=D-S_C$	8.1	3.0	2.5	1.5

%D.

Table 5 Profile-averaged values from verification of wave profile for Series 60.

Study	R_G	p_G	C_G	U_G	U_{G_C}
1 (grids 1-3)	0.62	1.4	0.60	2.6%	1.0%
2 (grids 2-4)	0.64	1.3	0.57	3.6%	1.4%

$\%\zeta_{max}$.

Table 6. Profile-averaged values from validation of wave profile for Series 60 – study 1 (grids 1-3).

	***E*%**	U_V%	U_D%	U_{SN}%
E=*D-S*	5.2	4.5	3.7	2.6
E_C=*D-*S_C	5.5	3.8	3.7	1.0

$\%\zeta_{max}$.

Table 7. Profile-averaged values from validation of wave profile for Series 60 – study 2 (grids 2-4).

	E%	U_V%	U_D%	U_{SN}%
E=*D-S*	5.5	5.1	3.7	3.6
E_C=*D-*S_C	6.6	3.9	3.7	1.4

$\%\zeta_{max}$.

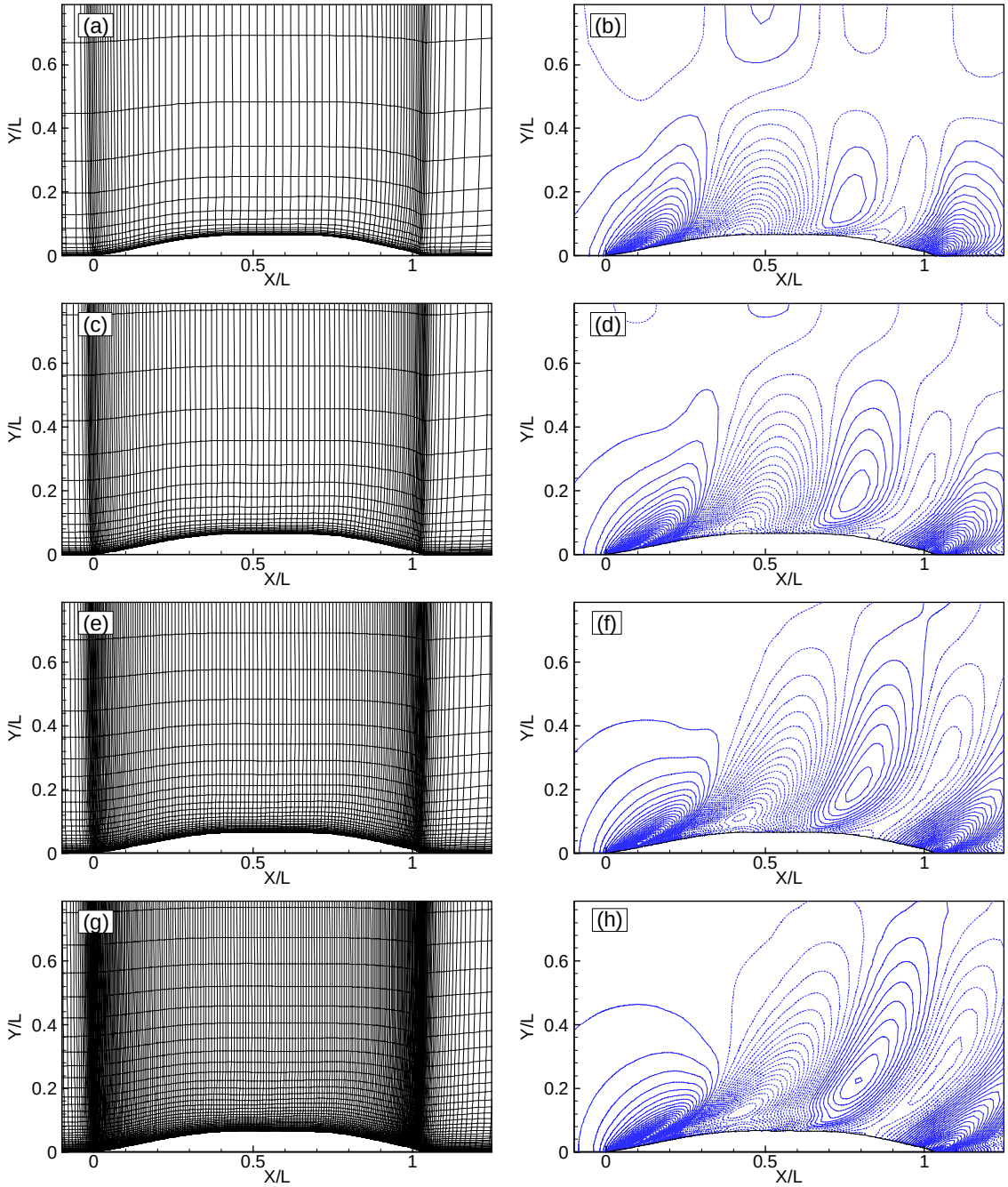

Figure 1. Grids and wave contours from verification and validation studies for Series 60: (a) and (b) coarsest - grid 4; (c) and (d) grid 3; (e) and (f) grid 2; and (g) and (h) finest - grid 1.

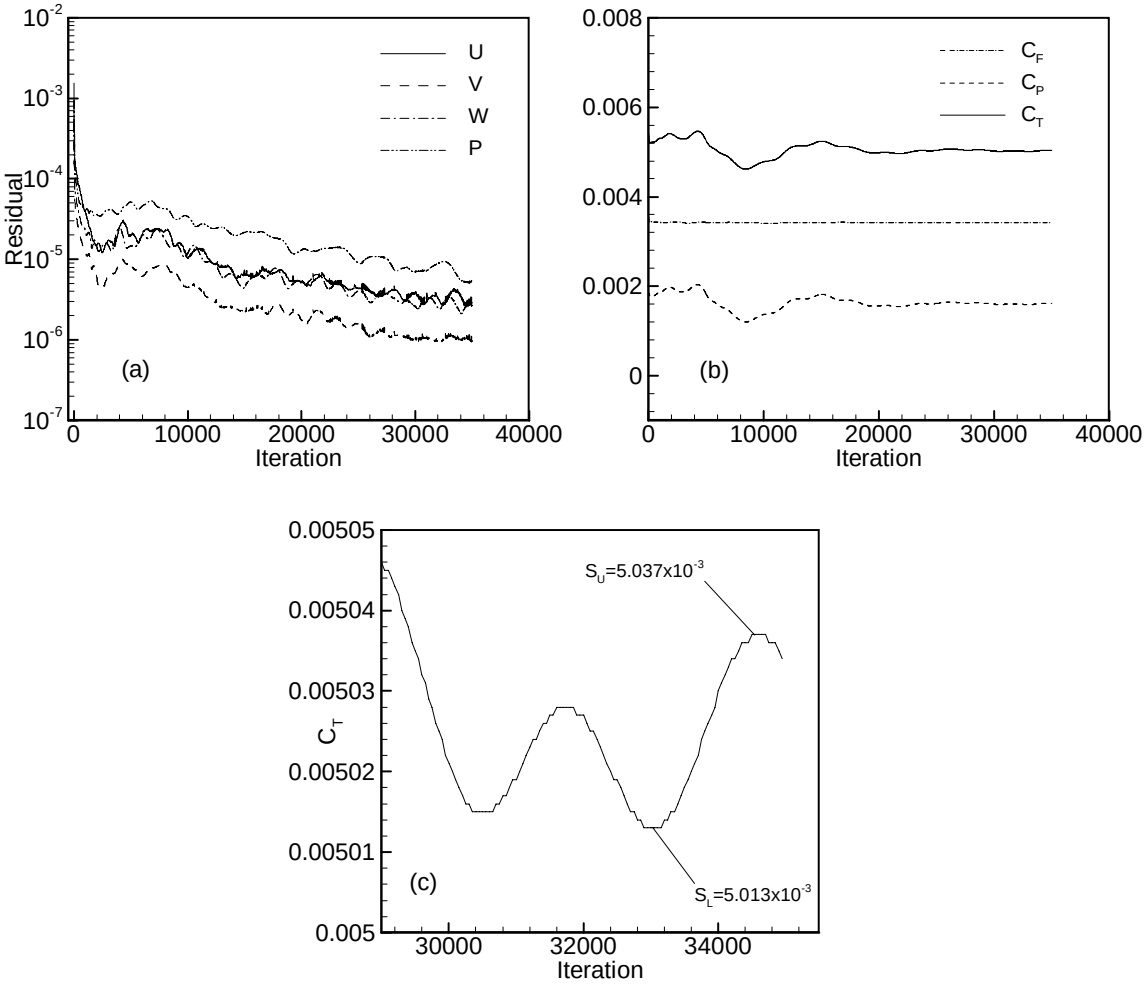

Figure 2. Iteration history for Series 60 on grid 1: (a) solution change, (b) ship forces - C_F, C_P, *and* C_T and (c) magnified view of total resistance C_T over last two periods of oscillation.

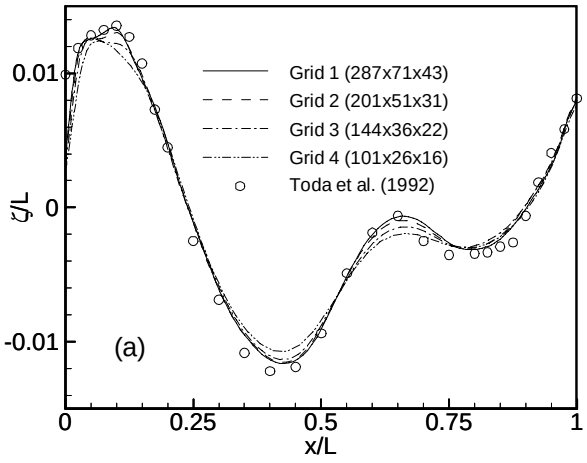

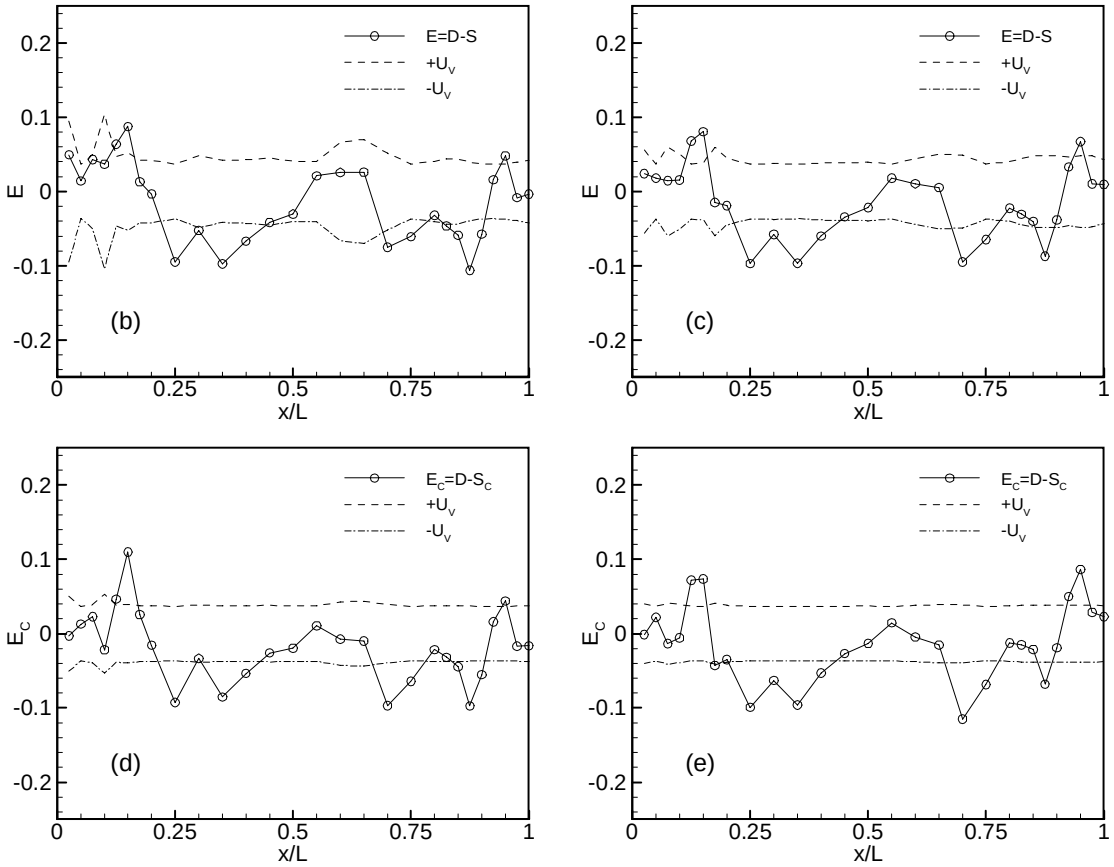

Figure 3. Wave profile for Series 60: (a) grid study; (b) and (d) validation using grids 2-4; and (c) and (e) validation using grids 1-3.